

Data-driven identification and analysis of the glass transition in polymer melts

Atreyee Banerjee, Hsiao-Ping Hsu, Kurt Kremer, and Oleksandra Kukharenko
Max Planck Institute for Polymer Research, Ackermannweg 10, 55128 Mainz, Germany
(Dated: November 28, 2022)

We propose a data-driven approach based on information about structural fluctuations of polymer chains, which clearly identifies the glass transition temperature T_g of polymer melts of weakly semiflexible chains. We use principal component analysis (PCA) with clustering to distinguish between liquid and glassy states and predict T_g in the asymptotic limit. Our method indicates that for temperatures approaching T_g from above it is sufficient to consider short molecular dynamics simulation trajectories, which just reach into the Rouse-like monomer displacement regime. The first eigenvalue of PCA and participation ratio show sharp changes around T_g . Our approach requires minimum user inputs and is robust and transferable.

Polymer materials in applications are usually in the glassy state. Upon cooling of a rubbery liquid polymer, dynamic properties such as viscosity or relaxation time increase drastically near the glass transition temperature (T_g) in a super-Arrhenius fashion [1–4] without any remarkable change in structural properties [3]. Despite enormous experimental and theoretical efforts [5–10], the nature of glass transition as well as the question of a precisely defined T_g still remain unclear [4, 11–14]. In computer simulations, T_g is often calculated from characteristic macroscopic properties, e.g. changes in the specific volume, density or in energy [14–16]. The increase in viscosity, equivalently of the terminal relaxation times, is commonly fitted to a Vogel-Fulcher-Tamann behavior which predicts a divergence at T_{VFT} [17], typically about 50° below the calorimetric T_g [18]. However, the observed value of T_g depends on the cooling rate and fitting procedures, which can lead to some ambiguities in comparison with experimental values [19, 20]. Unlike a sharp and distinct change in physical properties, most of the simulated glass transition temperatures are obtained from the bilinear fits (of specific volume, density or energy vs temperature) that somewhat depend on the fitting range. Thus reliable predictions of T_g are indeed challenging [12, 13, 21, 22].

Lately, attempts to link T_g with the molecular structure of polymeric materials draw more attention. Recent studies predict T_g by quantifying the changes in specific dihedral angles and transitions between states defined by those angles [13, 14] or by using averaged intra-chain properties [23]. A possibility to specify the structural properties of the glassy systems which can reflect changes in T_g is attractive, but it remains challenging and system specific. Machine learning (ML) methods hold a great promise to automatize the determination of structural descriptors from molecular simulation data. Recently, the application of ML to non-polymeric supercooled model liquids allowed to understand the connection between characteristic local structures and the slowing down of dynamical properties [24–29]. For polymer chains in a melt, the intra-chain properties associated with the chain connectivity and flexibility also play an important role in determining T_g . However, application of ML methods to determine structural changes

during the glass transition in polymer chains is limited [13, 30, 31].

In this letter, we use unsupervised data-driven methods to identify the glass transition of polymer melts containing weakly entangled polymer chains only by employing information about conformational fluctuations at different temperatures. We first analyse the combined data from different temperatures using principal component analysis (PCA) [32], followed by clustering and determine a clear signature of glass transition. Considering the simulation data within a finite observation time window up into the Rouse-like regime, we predict T_g in the asymptotic limit. We then employ the data-driven methods on individual temperature data separately. The non-monotonic variation of the magnitudes of leading eigenvalues and the participation ratio derived from PCA captures the signature of the glass transition. It also reflects a change in the nature of the fluctuations in the system. We apply these approaches to the simulation data of a coarse-grained polymer model [33] and compare estimates of T_g obtained from classical fitting of macroscopic properties with the new method.

In Ref. [33], Hsu and Kremer developed a new variant of bead-spring model [34, 35] for studying the glass transition of polymer melts [36, 37]. Molecular dynamics simulations of a bulk polymer melt containing $n_c = 2000$ semiflexible polymer chains of chain length $n_m = 50$ monomers with Kuhn length $\approx 2.66\sigma$ [38] were first performed in the NPT ensemble at $P \approx 0\epsilon/\sigma^3$ and constant T following a standard stepwise cooling protocol. After the step cooling, subsequent NVT runs up to $3 \times 10^4\tau$ were performed at each T to investigate the monomer mobility characterized by the mean square displacement $g_1(t)$ (for details see supplemental material (SM) [39], Sec. S-I, Fig. S1). In this letter, we mainly use simulation trajectories stored every 200τ in the time window between 200τ and $3 \times 10^4\tau$ (gray area in Fig. S1, SM) resulting in 150 frames per temperature.

The first estimate of glass transition temperature $T_g \approx 0.64\epsilon/k_B$ was determined from the volume change (Fig. 1a inset) [33]. We here adapt another approach to estimate T_g by performing a hyperbola fit [40] on the temperature-dependent density of polymer melt, $\rho(T) = c - a(T - T_0) - \frac{b}{2}(T - T_0 + \sqrt{(T - T_0)^2 + 4e^f})$,

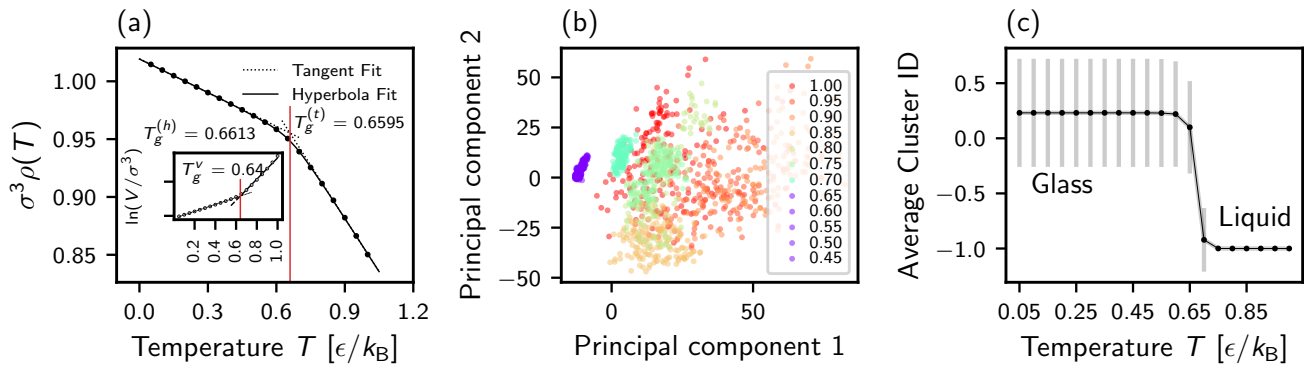


FIG. 1. (a) Conventional methods of estimating the glass transition temperature T_g : Density $\rho(T)$ and logarithm of volume, $\ln(V/\sigma^3)$ (in the inset), plotted versus T . Estimates of T_g via the two tangent (t) fits (dotted lines) at high and low T , hyperbola (h) fit (curve), and two linear fits (dashed lines in the inset) are indicated by vertical lines. (Data are taken from Ref. 33). (b-c) Data-driven determination of T_g . (b) Projections of concatenated data from all T for a randomly selected chain in the new reduced space determined using PCA. Each point in the plot corresponds to one chain's conformation at a given temperature at each time. Projections for $T > T_g$ are colored varying from red to green while they are in purple for $T < T_g$ (data shown for $T \geq 0.45$ for clarity). Note that the axis values in the PCA embedding don't correspond to a directly measurable physical quantity, rather could be viewed as a weighted linear combination of scaled input distances. (c) DBSCAN of the PCA projections. Results are averaged over all chains and the average cluster index (ID) is plotted versus T . The separation between the liquid and glass state becomes sharper if we use median instead of mean (see SM, Fig. S5).

where c , T_0 , a , b and f are fitting parameters. T_g is either defined by $T_g = T_0$ or the intersection point of the two tangents drawn at the high and the low temperature. Both definitions give the identical, more precise estimates of $T_g = 0.660(4)\epsilon/k_B$ as shown in Fig. 1a. The methods of predicting T_g based on the macroscopic properties such as density or volume are thus sensible to the fitting protocols since no sharp transition around T_g is observed. Therefore, we propose here an alternative data-driven approach to gain insight into glass transition with a minimum a priori knowledge about the system and user input.

The analysis workflow consists of two independent parts (a sketch is given in SM, Sec. S-II). Both identify the same T_g , but treat the data differently (using combined information from all 20 temperatures or individual information from each temperature) and use different properties for the predictions. To identify changes in the studied systems, we first define possible descriptors: sets of all pairwise internal distances for a single chain. They are well suited to describe conformational fluctuations of individual polymer chains. Then we apply principal component analysis (PCA) [32] to the high-dimensional descriptor space. The method relies on purely structural information without any a priori knowledge of dynamical correlations. A data matrix $\mathbf{X} \in \mathbb{R}^{L \times M}$ is used to represent a data set, which is standardised column-wise, i.e., it has mean of 0 and variance of 1. Here L is the number of descriptors (e.g. the intra-chain distances of a single chain of $n_m = 50$ monomers: $L = n_m \times (n_m - 1)/2 = 1225$ [41]) and M is the number of observations (i.e. time frames multiplied by number of temperatures for the first

part, $M = 150 \times 20 = 3000$, and time frames at each individual temperature, $M = 150$, for the second part of analysis). PCA is done by first calculating the covariance matrix $C = \mathbf{X}^T \mathbf{X}$ (C is symmetric and positively defined). Then the pairs of eigenvalues λ_i and eigenvectors \mathbf{v}_i , for $i = 1, 2, 3, \dots, \min(L, M)$ are calculated for the covariance matrix and sorted in decreasing order of eigenvalues. The original data set is then projected to the new orthogonal basis.

First, we perform PCA on a randomly selected single chain using the internal distance vectors over time concatenated for all temperatures. In this way we construct the new basis formed by eigenvectors \mathbf{v}_i containing information about fluctuations of internal distances at all temperatures. The distance vector of the chain at each frame and temperature is projected independently on this new basis. Thus, projections in the new PCA space can be viewed as linear combinations of input distances. Already in two-dimensional projection, one could clearly differentiate between two states (Fig. 1b), which occur roughly around the glass transition temperature $T_g \approx 0.65\epsilon/k_B$ (Fig. 1a). The scatter of the PCA projection qualitatively changes at and below $0.65\epsilon/k_B$ indicating the onset of a different state.

To confirm that the separation between liquid and glassy state is consistent for all chains in the melt and to obtain a general estimate of the temperature at which this separation occurs, we perform PCA for each chain separately, followed by density-based spatial clustering of applications with noise (DBSCAN) [42] for each projection in four dimensional space of leading principal components (PCs). DBSCAN groups together the data points that

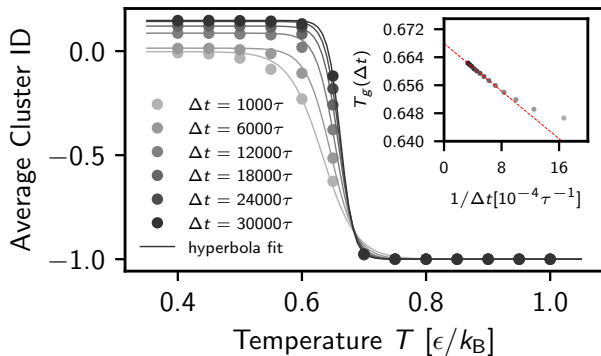


FIG. 2. DBSCAN for different selected observation time windows Δt , as indicated. The curves give the best hyperbola fit $g(T)$ going through the data. The inflection point of $g(T)$ shown in the inset gives the estimate of $T_g(\Delta t)$ at each Δt . Extrapolating to $\Delta t \rightarrow \infty$, we obtain $T_g \approx 0.6680\epsilon/k_B$.

are close based on two hyperparameters: the Euclidean distance ($\epsilon_d = 0.3$) to create a neighbourhood and the minimum number of points ($NN = 40$) to form a dense region. A discussion of the choice of DBSCAN parameters is given in the SM, Sec. S-III. In Fig. 1c the averaged cluster indices over all the 2000 chains are plotted. The change in cluster indices at $T = 0.65\epsilon/k_B$ is prominent with the separation of the glassy state as a cluster and the liquid state as noise.

For comparison, a similar analysis is applied to two classical physical descriptors, radius of gyration R_g and end-to-end distances R_e , since they also contain the information about the intra-chain distances. As expected there is no clear signature of separation around T_g compared to the corresponding PCA space given in Fig. 1b (see Sec. S-II in SM).

Results of the averaged DBSCAN cluster indices for different observation time windows Δt are shown in Fig. 2. We see that the transition from liquid to glassy state becomes sharper with the increase of observation time window. To quantify that we interpolate the data by a hyperbolic tangent function $g(T) = C(\Delta t)(1 - \tanh(sT - d))/2 - 1$, where s and d are the fitting parameters, $C(\Delta t)$ is the gap between the two states at $T \gg T_g$ and $T \ll T_g$, respectively. The inflection point of $g(T)$ gives the estimate of $T_g(\Delta t)$ depending on Δt . Taking into account this finite-time effect, we plot the estimates of $T_g(\Delta t)$ versus $1/\Delta t$ in the inset of Fig. 2. We find a remarkable linear dependency, which allows for an extrapolation to $\Delta t \rightarrow \infty$ and obtain $T_g \approx 0.6680\epsilon/k_B$ as a best asymptotic estimate of T_g . This is in excellent agreement with the classical analysis of the temperature-dependent density.

Here, we performed PCA on a single chain, followed by taking an average over all chains in the system. Performing PCA on 2000 chains combined, we only observe the same Gaussian-like distribution for all temperatures

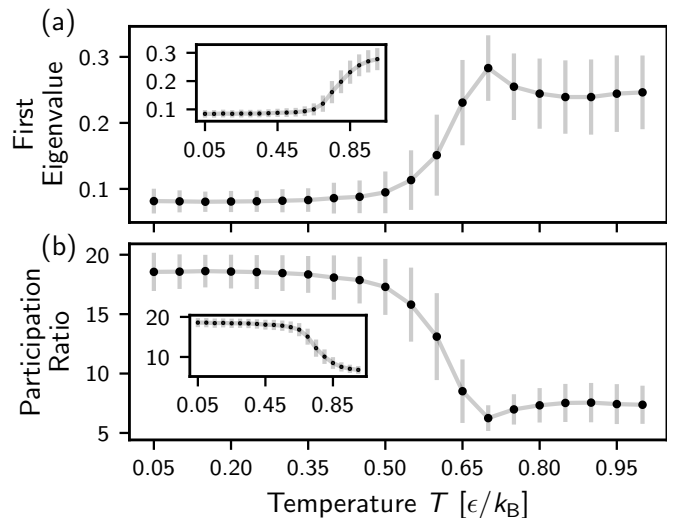


FIG. 3. Analysis of each temperature independently. (a) Mean values including error bars of the magnitude of first eigenvalues and (b) the participation ratio. The short time results are shown in the insets.

within fluctuations (see SM, Fig. S8).

In order to interpret the obtained PCs, we calculate the correlation between input features and the corresponding PCs (see SM, Sec. S-VI). The mostly-correlated distances vary with different chains, with no clear signature of any characteristic distance. However, the leading PCs are related with physically motivated measures such as R_g , R_e . The glass transition is often viewed as the onset of ergodicity breaking. Above T_g all states are accessible to the system, while below T_g the system is arrested. Therefore, we expect the dissimilarity between low and high temperature regimes at or around T_g : giving rise to the jump in the average cluster indices. Our result shows a signature of ergodicity breaking for each chain at the same temperature — we report that as T_g . A similar signature of ergodicity breaking is reported recently using Jensen–Shannon divergence metric for homopolymers [13].

In the following, we challenge our approach and perform PCA for individual chains, but at different temperatures independently. In this way, no information of individual chain conformations from other temperatures is accessible. Resulting projections are shown in SM, Fig. S11. Notably, for majority of chains in the melt, we could observe the change from a completely random distribution of points in the projection to more “clustered” with the decrease of T from $T = 1.0\epsilon/k_B$. The observed behaviour can be quantified by the magnitude of the eigenvalues of PCA. In general, this magnitude is not a uniform value for independently projected data, but in our case all distances are standardised. Thus, we could average over the first eigenvalue for all projections (see Fig. 3a).

As a more general criterion, we use the participation ratio (PR) defined at each temperature as $PR = (\sum_{i=1}^k \lambda_i)^2 / \sum_{i=1}^k \lambda_i^2$ (see Fig. 3b). The leading $k = 25$

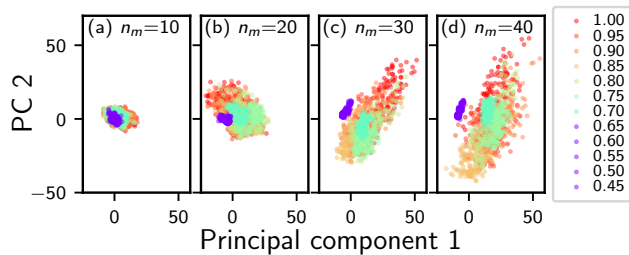


FIG. 4. PCA projections of concatenated data from all temperatures for subchains of lengths $n_m = 10$ (a), 20 (b), 30 (c), and 40 (d) for a randomly selected chains. The separation between low-temperature glassy states and high-temperature liquid states becomes less prominent with the decrease of sub-chain length.

eigenvalues from $\min(L, M)$ eigenvalues are counted to preserve at least 80% data fluctuations in PCs. Results are averaged over all chains, deviations are shown as errorbar. The increase in the magnitude of the first eigenvalue or the decrease in PR on approaching T_g can be related to an appearance of state separation in the system and change in a local structure as some recent studies suggest [13, 14]. We argue that a prominent change in the monotonic behaviour of PR (or the first eigenvalue) is connected with a change in the nature of the fluctuations in the system: from local configurational rearrangements above T_g to only vibrations along the chain below T_g (similar to observations in metallic glasses [43]). As a result, more dimensions are needed to describe the random motion below T_g . With this method, one can perform PCA on simulation trajectories at each temperature and monitor the eigenvalues and PR. Once we observe the non-monotonic change in both quantities around T_g , further simulations at lower temperatures are not required. To test the hypothesis about local structural changes above T_g , we perform the same analysis on simulation trajectories within a relatively short time window between 0.2τ and 20τ (blue area in Fig. S1). Results are shown in the inset in Fig. 3, respectively. We no longer see the non-monotonic signature around T_g since chains remain in their initial conformations within 1σ fluctuation in such a small time window. Projections of short time data from individual temperature are given in SM, Fig. S12.

Furthermore, $T_g(N)$ approaches $T_g(N \rightarrow \infty)$ for $N > N_e$, where N_e is the entanglement length [44, 45]. To see how and whether this also applies to subchains below and around N_e , we performed the PCA analysis both on concatenated and independent data from different temperatures for subchains of lengths $n_m = 10, 20, 30, 40$ monomers. [46] PCA projections of simulation data concatenated from all temperatures for subchains of various different chain lengths in a randomly selected chain are shown in Fig. 4. The averaged results of DBSCAN for all chains of different subchain lengths are shown in Fig. 5a.

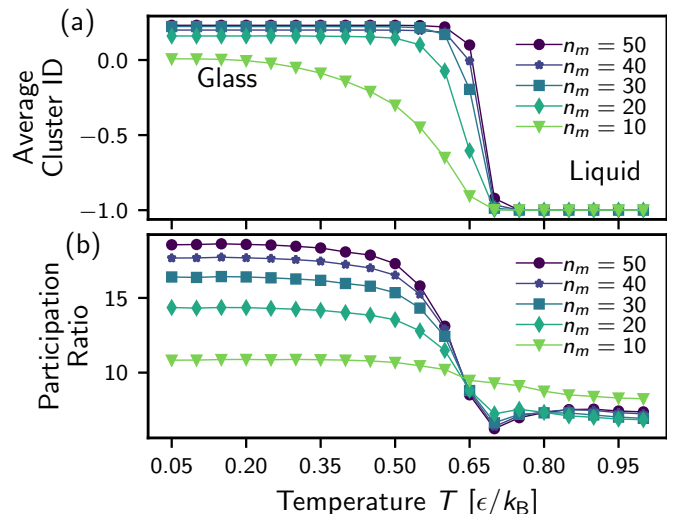


FIG. 5. (a) Averaged DBSCAN indices for PCA projections of concatenated data from all temperatures. (b) PR for independent PCA projections of data from individual temperatures. Analyses are done for subchains of lengths $n_m = 10, 20, 30,$ and 40 . Data for $n_m = 50$ are also shown for comparison (see Fig. 1c and Fig. 3b). The error bars are not shown for clarity.

The separation becomes less prominent with a decrease in subchain length and the inflection point shifts to lower temperatures, as expected [44, 45].

We also analysed the data at individual temperatures for different selected subchain lengths. Results of the participation ratio (PR) are presented in Fig. 5b. Furthermore, the contributions from the low eigenvalues of PCA as considered in Ref. [30] are evaluated as well. Details are given in SM, Sec. S-IX. For $n_m = 10$, we do not observe a clear signature of change in PR. There is no strong difference between the liquid and glassy state seen in PCA projections (see Fig. 4). The results obtained for the full chains (Fig. 1b) are reproduced for $n_m \geq 30$, namely above $N_e = 28$ [38]. This suggests that the same methodology can be applied for much longer chains by using subchains (preferably longer than N_e) without facing the problem of increasing input dimensionality.

In summary, we propose a new approach for determining the glass transition temperature from molecular dynamics simulation data. The proposed data-driven protocol requires minimum input parameters and predicts T_g in a robust and transferable fashion. It is able to identify an extrapolated T_g for infinite simulation time and is in a good agreement with the conventional protocols. The method can be applied to a wide range of systems with microscopic/atomistic information. Further work in this direction is in progress.

ACKNOWLEDGMENTS

We acknowledge open-source packages Numpy [47], Matplotlib [48], Scikit-learn [49] used in this work. The au-

thors thank Michael A. Webb, Saikat Chakraborty and Daniele Coslovich for insightful discussion. The authors also thank Aysenur Iscen and Denis Andrienko for critical reading of the manuscript.

-
- [1] C. Angell, Perspective on the glass transition, *J. Phys. Chem. Solids* **49**, 863 (1988).
- [2] C. A. Angell, Formation of glasses from liquids and biopolymers, *Science* **267**, 1924 (1995).
- [3] K. Binder, J. Baschnagel, and W. Paul, Glass transition of polymer melts: test of theoretical concepts by computer simulation, *Prog. Polym. Sci.* **28**, 115 (2003).
- [4] L. Berthier and G. Biroli, Theoretical perspective on the glass transition and amorphous materials, *Rev. Mod. Phys.* **83**, 587 (2011).
- [5] T. R. Kirkpatrick, D. Thirumalai, and P. G. Wolynes, Scaling concepts for the dynamics of viscous liquids near an ideal glassy state, *Phys. Rev. A* **40**, 1045 (1989).
- [6] W. Gotze and L. Sjogren, Relaxation processes in supercooled liquids, *Rep. Prog. Phys.* **55**, 241 (1992).
- [7] L. F. Cugliandolo and J. Kurchan, Analytical solution of the off-equilibrium dynamics of a long-range spin-glass model, *Phys. Rev. Lett.* **71**, 173 (1993).
- [8] P. Wolynes, Entropy crises in glasses and random heteropolymers, *J. Res. Natl. Inst. Stan.* **102**, 187 (1997).
- [9] S. Sastry, P. G. Debenedetti, and F. H. Stillinger, Signatures of distinct dynamical regimes in the energy landscape of a glass-forming liquid, *Nature* **393**, 554 (1998).
- [10] J. Dudowicz, K. F. Freed, and J. F. Douglas, The glass transition temperature of polymer melts, *J. Phys. Chem. B* **109**, 21285 (2005).
- [11] G. Biroli and J. P. Garrahan, Perspective: The glass transition, *J. Chem. Phys.* **138**, 12A301 (2013).
- [12] K.-H. Lin, L. Paterson, F. May, and D. Andrienko, Glass transition temperature prediction of disordered molecular solids, *Npj Comput. Mater.* **7** (2021).
- [13] T. Jin, C. W. Coley, and A. Alexander-Katz, Molecular signatures of the glass transition in polymers, *Phys. Rev. E* **106** (2022).
- [14] F. Godey, A. Fleury, and A. Soldera, Local dynamics within the glass transition domain, *Sci Rep* **9** (2019).
- [15] P. G. Debenedetti and F. H. Stillinger, Supercooled liquids and the glass transition, *Nature* **410**, 259 (2001).
- [16] B. Schnell, H. Meyer, C. Fond, J. P. Wittmer, and J. Baschnagel, Simulated glass-forming polymer melts: Glass transition temperature and elastic constants of the glassy state, *Eur. Phys. J. E* **34** (2011).
- [17] A. Soldera and N. Metatla, Glass transition of polymers: Atomistic simulation versus experiments, *Phys. Rev. E* **74** (2006).
- [18] J. Zhao and G. B. McKenna, Temperature divergence of the dynamics of a poly(vinyl acetate) glass: Dielectric vs. mechanical behaviors, *J. Chem. Phys.* **136**, 154901 (2012).
- [19] N. Yasoshima, M. Fukuoka, H. Kitano, S. Kagaya, T. Ishiyama, and M. Gemmei-Ide, Diffusion-controlled recrystallization of water sorbed into poly(meth)acrylates revealed by variable-temperature mid-infrared spectroscopy and molecular dynamics simulation, *J. Phys. Chem. B* **121**, 5133 (2017).
- [20] F. Godey, A. Fleury, A. Ghoufi, and A. Soldera, The extent of the glass transition from molecular simulation revealing an overcrank effect, *J. Comput. Chem.* **39**, 255 (2017).
- [21] W. Chu, M. A. Webb, C. Deng, Y. J. Colón, Y. Kambe, S. Krishnan, P. F. Nealey, and J. J. de Pablo, Understanding ion mobility in p2vp/nmp+i- polymer electrolytes: A combined simulation and experimental study, *Macromolecules* **53**, 2783 (2020).
- [22] C. Deng, M. A. Webb, P. Bennington, D. Sharon, P. F. Nealey, S. N. Patel, and J. J. de Pablo, Role of molecular architecture on ion transport in ethylene oxide-based polymer electrolytes, *Macromolecules* **54**, 2266 (2021).
- [23] D. L. Baker, M. Reynolds, R. Masurel, P. D. Olmsted, and J. Mattsson, Cooperative intramolecular dynamics control the chain-length-dependent glass transition in polymers, *Phys. Rev. X* **12** (2022).
- [24] S. S. Schoenholz, E. D. Cubuk, E. Kaxiras, and A. J. Liu, Relationship between local structure and relaxation in out-of-equilibrium glassy systems, *P. Natl. Acad. Sci. USA* **114**, 263 (2016).
- [25] V. Bapst, T. Keck, A. Grabska-Barwińska, C. Donner, E. D. Cubuk, S. S. Schoenholz, A. Obika, A. W. R. Nelson, T. Back, D. Hassabis, and P. Kohli, Unveiling the predictive power of static structure in glassy systems, *Nat. Phys.* **16**, 448 (2020).
- [26] E. Boattini, S. Marín-Aguilar, S. Mitra, G. Foffi, F. Smalenburg, and L. Filion, Autonomously revealing hidden local structures in supercooled liquids, *Nat. Commun.* **11** (2020).
- [27] E. Boattini, F. Smalenburg, and L. Filion, Averaging local structure to predict the dynamic propensity in supercooled liquids, *Phys. Rev. Lett.* **127**, 088007 (2021).
- [28] P. S. Clegg, Characterising soft matter using machine learning, *Soft Matter* **17**, 3991 (2021).
- [29] D. Coslovich, R. L. Jack, and J. Paret, Dimensionality reduction of local structure in glassy binary mixtures, *J. Chem. Phys.* **157**, 204503 (2022).
- [30] N. Iwaoka and H. Takano, Conformational fluctuations of polymers in a melt associated with glass transition, *J. Phys. Soc. Jpn.* **86**, 035002 (2017).
- [31] Y. Shimizu, T. Kurokawa, H. Arai, and H. Washizu, Higher-order structure of polymer melt described by persistent homology, *Sci Rep* **11** (2021).
- [32] H. Abdi and L. J. Williams, Principal component analysis, *WIREs Comp Stat* **2**, 433 (2010).
- [33] H.-P. Hsu and K. Kremer, A coarse-grained polymer model for studying the glass transition, *J. Chem. Phys.* **150**, 091101 (2019); **150**, 159902 (2019).
- [34] K. Kremer and G. S. Grest, Dynamics of entangled linear polymer melts: a molecular-dynamics simulation, *J. Chem. Phys.* **92**, 5057 (1990).
- [35] K. Kremer and G. S. Grest, Simulations for structural and dynamic properties of dense polymer systems, *J. Chem. Soc., Faraday Transactions* **88**, 1707 (1992).

- [36] W.-S. Xu, J. F. Douglas, and X. Xu, Molecular dynamics study of glass formation in polymer melts with varying chain stiffness, *Macromolecules* **53**, 4796 (2020).
- [37] W.-S. Xu, J. F. Douglas, and X. Xu, Role of cohesive energy in glass formation of polymers with and without bending constraints, *Macromolecules* **53**, 9678 (2020).
- [38] H.-P. Hsu and K. Kremer, Static and dynamic properties of large polymer melts in equilibrium, *J. Chem. Phys.* **144**, 154907 (2016).
- [39] See Supplemental material at URL will be inserted by the publisher.
- [40] P. N. Patrone, A. Dienstfrey, A. R. Browning, S. Tucker, and S. Christensen, Uncertainty quantification in molecular dynamics studies of the glass transition temperature, *Polymer* **87**, 246 (2016).
- [41] Due to correlated motions of neighboring monomers the intra-chain distance space can be reduced by skipping some distances. We discuss this in more details in SM, Sec. S-VIII.
- [42] M. Ester, H.-P. Kriegel, J. Sander, and X. Xu, A density-based algorithm for discovering clusters in large spatial databases with noise, in *Proceedings of the Second International Conference on Knowledge Discovery and Data Mining*, KDD'96 (AAAI Press, 1996) pp. 226–231.
- [43] H. L. Smith, C. W. Li, A. Hoff, G. R. Garrett, D. S. Kim, F. C. Yang, M. S. Lucas, T. Swan-Wood, J. Y. Y. Lin, M. B. Stone, D. L. Abernathy, M. D. Demetriou, and B. Fultz, Separating the configurational and vibrational entropy contributions in metallic glasses, *Nat. Phys.* **13**, 900 (2017).
- [44] K. O'Driscoll and R. A. Sanayei, Chain-length dependence of the glass transition temperature, *Macromolecules* **24**, 4479 (1991).
- [45] A. Y. Liu, H. Emamy, J. F. Douglas, and F. W. Starr, Effects of chain length on the structure and dynamics of semidilute nanoparticle–polymer composites, *Macromolecules* **54**, 3041 (2021).
- [46] We tested different ways of selecting subchains: including or excluding end-parts. There was no influence on the obtained results. Here we show results for subchains selected from one end of the chain.
- [47] C. R. Harris, K. J. Millman, S. J. van der Walt, R. Gommers, P. Virtanen, D. Cournapeau, E. Wieser, J. Taylor, S. Berg, N. J. Smith, R. Kern, M. Picus, S. Hoyer, M. H. van Kerkwijk, M. Brett, A. Haldane, J. F. del Río, M. Wiebe, P. Peterson, P. Gérard-Marchant, K. Sheppard, T. Reddy, W. Weckesser, H. Abbasi, C. Gohlke, and T. E. Oliphant, Array programming with NumPy, *Nature* **585**, 357 (2020).
- [48] J. D. Hunter, Matplotlib: A 2d graphics environment, *Comput Sci Eng* **9**, 90 (2007).
- [49] F. Pedregosa, G. Varoquaux, A. Gramfort, V. Michel, B. Thirion, O. Grisel, M. Blondel, P. Prettenhofer, R. Weiss, V. Dubourg, J. Vanderplas, A. Passos, D. Cournapeau, M. Brucher, M. Perrot, and E. Duchesnay, Scikit-learn: Machine learning in python, *J. Mach. Learn. Res.* **12**, 2825–2830 (2011).